HHS Public Access

Author manuscript

Ann Biomed Eng. Author manuscript; available in PMC 2016 November 01.

Published in final edited form as:

Ann Biomed Eng. 2015 November ; 43(11): 2722–2734. doi:10.1007/s10439-015-1327-2.

Modeling of Tracer Transport Delays for Improved Quantification of Regional Pulmonary ^{18}F-FDG Kinetics, Vascular Transit Times, and Perfusion

Tyler J. Wellman, PhD[1] **[Postdoctoral Research Fellow]**, **Tilo Winkler, PhD**[2] **[Assistant Professor]**, and **Marcos F. Vidal Melo, MD, PhD**[3] **[Associate Professor]**

[1]Department of Anesthesia, Critical Care and Pain Medicine, Massachusetts General Hospital and Harvard Medical School, Boston, MA

[2]Department of Anesthesia, Critical Care and Pain Medicine, Massachusetts General Hospital and Harvard Medical School, Boston, MA

[3]Department of Anesthesia, Critical Care and Pain Medicine, Massachusetts General Hospital and Harvard Medical School, Boston, MA

Abstract

^{18}F-FDG-PET is increasingly used to assess pulmonary inflammatory cell activity. However, current models of pulmonary ^{18}F-FDG kinetics do not account for delays in ^{18}F-FDG transport between the plasma sampling site and the lungs. We developed a three-compartment model of ^{18}F-FDG kinetics that includes a delay between the right heart and the local capillary blood pool, and used this model to estimate regional pulmonary perfusion. We acquired dynamic ^{18}F-FDG scans in 12 mechanically ventilated sheep divided into control and lung injury groups (n=6 each). The model was fit to tracer kinetics in three isogravitational regions-of-interest to estimate regional lung transport delays and regional perfusion. ^{13}NN bolus infusion scans were acquired during a period of apnea to measure regional perfusion using an established reference method. The delayed input function model improved description of ^{18}F-FDG kinetics (lower Akaike Information Criterion) in 98% of studied regions. Local transport delays ranged from 2.0–13.6s, averaging 6.4±2.9s, and were highest in non-dependent regions. Estimates of regional perfusion derived from model parameters were highly correlated with perfusion measurements based on ^{13}NN-PET (R^2=0.92, p<0.001). By incorporating local vascular transports delays, this model of pulmonary ^{18}F-FDG kinetics allows for simultaneous assessment of regional lung perfusion, transit times, and inflammation.

Keywords

plasma input function; tracer kinetics; capillary transit times; positron emission tomography

Address for Correspondence: Marcos F. Vidal Melo, MD, PhD, Department of Anesthesia, Critical Care, and Pain Medicine, Massachusetts General Hospital, 55 Fruit St, Boston, MA 02114. mvidalmelo@partners.org, Phone: 617-726-4654, Fax: n/a.

Introduction

Positron emission tomography (PET) imaging of 2-deoxy-2-[^{18}F]-fluoro-D-glucose (^{18}F-FDG) in the lungs has been increasingly used to investigate changes in glucose metabolism underlying various lung diseases. In the acute respiratory distress syndrome (ARDS), ^{18}F-FDG-PET is used to assess the metabolic activation associated with lung inflammation, which reflects primarily the infiltration and activation of neutrophils.[6, 15, 18, 23, 31] Several analytical methods, including the Patlak analysis,[25] Sokoloff model,[36] and four-compartment model,[32] have been applied to quantify ^{18}F-FDG transport and trapping within lung tissue. Current techniques for defining the lung plasma input function that is required for these models include manual sampling of blood in the pulmonary artery[4] or systemic artery,[26] and imaging of a region-of-interest characterizing the right heart blood pool with calibration using manual samples.[33]

A major assumption underlying those approaches is that the plasma activity assessed at the sampling site (e.g., the arteries or right heart) is an accurate representation of the plasma activity within the pulmonary capillary blood pool, the site of tracer entry into the tissue. However, the vascular transport of intravenously infused ^{18}F-FDG gives rise to a delay between the sampling site and the pulmonary capillary blood pool. In the lungs, transport delays are likely heterogeneous, given the previously described heterogeneity of pulmonary capillary transit times.[41] Such transport delays have long been recognized and modeled in other applications of PET such as myocardial perfusion imaging,[16, 24] assessment of cerebral blood flow[37] and metabolism,[12, 45] and ^{15}O-water imaging of pulmonary blood flow.[29] In contrast, analyses of pulmonary ^{18}F-FDG kinetics have not yet accounted for delays in the plasma input function,[4, 8, 32] potentially biasing estimates of parameters describing pulmonary ^{18}F-FDG uptake. To date, no study has examined the magnitude of this delay or its effect on estimates of pulmonary ^{18}F-FDG kinetics parameters. Moreover, the ability to assess delays in ^{18}F-FDG transport may allow for regional quantification of pulmonary capillary transit times and perfusion, key physiologic parameters which may be altered in disease.[35, 39]

In this study, we incorporate an input function delay into the standard three-compartment model of pulmonary ^{18}F-FDG kinetics. This new model – hereafter referred to as the delayed input function model – includes a delay of the plasma function to account for tracer transport time between the right heart and the local capillary blood pool. The model is compared with the standard three-compartment model without a delay – herein referred to as the right heart input function model. In addition, we demonstrate a novel method to estimate local pulmonary perfusion using the delayed input function model parameters. In two groups of mechanically ventilated sheep with healthy or acutely injured lungs, we aimed to: (1) examine distributions of the regional input function delay between the right heart and lung regions-of-interest; (2) compare values of ^{18}F-FDG kinetics parameters and measures of model goodness-of-fit between the right heart and delayed input function models; and (3) compare estimates of regional perfusion derived from parameters of the new model with those of a reference ^{13}NN-PET technique.

Materials and Methods

Animal Preparation

The protocols of this study were approved by the Subcommittee on Research Animal Care of the Massachusetts General Hospital. Twelve sheep (21.7±2.0 kg) were anesthetized, intubated and mechanically ventilated. Femoral artery, internal jugular vein and pulmonary artery catheters were inserted. Anesthesia was maintained with a continuous infusion of ketamine and propofol titrated to heart rate and blood pressure, and intermittent boluses of fentanyl. Paralysis was established with a bolus of pancuronium (0.1 mg/kg) at induction and repeated every 90 min (0.02–0.04 mg/kg).

Study Groups

We studied two groups of 6 supine mechanically ventilated sheep. In the Control group, we aimed to investigate normal physiological conditions; sheep were mechanically ventilated with a volume controlled mode, with tidal volume (V_T) set to 8 ml/kg, positive end-expiratory pressure (PEEP) of 0 cmH_2O, inspired oxygen fraction (F_IO_2) initially set to 0.3 and adjusted to maintain arterial oxygen saturation >90%, inspiratory-to-expiratory ratio I:E=1:2, and respiratory rate initially at 28 breaths/min and adjusted to maintain the arterial carbon dioxide partial pressure (P_aCO_2) between 32–45 mmHg. Animals were imaged after 20 min of mechanical ventilation to ensure steady-state conditions. For the Lung Injury group, we studied an ARDS model combining unilateral surfactant depletion[8] with mild endotoxemia[6] in order to produce varying degrees of regional inflammation as well as redistribution of perfusion. In each animal, a tracheotomy was performed and a left-sided double-lumen endobronchial tube was placed. While ventilating the right lung with F_IO_2=1, left lung surfactant depletion was produced by alveolar saline lavage. Starting from the supine position, warm saline (∼400 ml) was instilled in the left bronchus at a pressure of ∼30 cmH_2O and then drained by gravity. After three aliquots, animals were switched to the prone position for another three aliquots to homogenize lavage of ventral and dorsal lung. The double-lumen endobronchial tube was then replaced by a regular endotracheal tube and ventilation of both lungs was performed for 4 h with PEEP=10 cmH_2O, F_IO_2=0.6, V_T adjusted to a plateau pressure of 30 cmH_2O (V_T=13.4±3.5 ml/kg), I:E=1:2, and respiratory rate adjusted to normocapnia. During this ventilation period, sheep received a continuous intravenous infusion of endotoxin (10 $ng{\cdot}kg^{-1}{\cdot}min^{-1}$, Escherichia coli O55:B5, List Biological Laboratories Inc, California).

PET Imaging Protocols

For all PET scans, sheep were positioned supine in the camera (Scanditronix PC4096, GE Healthcare, Milwaukee, WI) with the most caudal slice adjacent to the diaphragm dome. The camera collected 15 transverse slices of 6.5 mm thickness over a 9.7-cm-long axial field. The following PET scans were acquired after 20 minutes of mechanical ventilation in the Control group or after 4 h ventilation in the Lung Injury group.

1. Transmission scans: obtained during 10 minutes of continuous breathing using a rotating pin-source of ^{68}Ge to correct PET emission scans for tissue attenuation and

to measure lung density.[28] These scans were processed as previously described to construct images of average fractional gas content (F_{GAS}).[14]

2. ^{13}NN bolus infusion emission scans: obtained as previously described to measure regional perfusion.[38, 43] Images consisted of 22 frames (8×2.5 s, 10×10 s, and 4×30 s). In brief, simultaneous with the start of imaging, a bolus of ^{13}NN (∼1000 MBq) dissolved in 40 mL saline was injected into the jugular vein at the beginning of 60 s of apnea. Due to its low solubility in water (partition coefficient water/air = 0.018 at 37°C), virtually all ^{13}NN in the blood diffuses into alveoli at first pass in aerated lung units, and ^{13}NN activity accumulates in proportion to regional blood flow. After 60 s, mechanical ventilation was resumed to remove ^{13}NN from the lungs over 10 minutes of washout.

3. ^{18}F-FDG emission scans: acquired immediately subsequent to ^{13}NN washout. ^{18}F-FDG (∼200 MBq dissolved in 8 mL saline) was infused at a constant rate over 60 s through the jugular catheter. Simultaneous with the start of infusion, a dynamic PET scan was started, consisting of 37 sequential frames (9×10 s, 4×15 s, 1×30 s, 7×60 s, 15×120 s, 1×300 s) over 45 minutes. Pulmonary arterial blood was sampled at 5.5, 9.5, 25, 37, and 42.5 minutes, and plasma ^{18}F-FDG concentration was measured in a well-counter cross-calibrated with the PET camera.[33]

PET images were reconstructed with voxel size of 2×2×6.5 mm using a convolution backprojection algorithm. Images were decay corrected to the beginning of tracer infusion and filtered in-plane with a circular moving average filter of diameter 12 mm and along the z-axis with a 2-point moving average filter. Each frame consisted of a 128×128×14 matrix with an effective volumetric resolution of 1.66 cm^3.

Definition of Lung Fields for Analysis

Volumetric masks of the imaged lung field were delineated by: (1) including all voxels with F_{GAS}>0.5; (2) adding perfused but poorly aerated lung regions viewed in the ^{13}NN infusion scan; and (3) manually refining masks to exclude the trachea, two main bronchi, and major blood vessels. Regions of interest (ROIs) were defined by dividing the lung field along the gravitational (i.e., ventral-dorsal) axis into three regions of equal height.

Delayed Input Function Model of Pulmonary ^{18}F-FDG Kinetics

In previous applications where the three-compartment model was used to describe pulmonary ^{18}F-FDG kinetics, the activity in the plasma compartment of the lungs was assumed to be equal to that at the blood sampling site.[4, 26, 33] We developed a modified version of this model (i.e., the delayed input function model; Fig. 1) wherein the local lung plasma concentration ($C_p[t]$) is represented by a delayed version of the image-derived plasma function measured in the right heart ($C_{RH}[t-t_{delay}]$) and calibrated with manual samples, as previously described.[33] For a given value of t_{delay}, $C_{RH}[t-t_{delay}]$ was computed by linear interpolation between measured points. This delay represents the time required for the tracer to travel from the right heart to a lung ROI, and is a function of the regional vascular volume between the right heart and the pulmonary capillaries, as well as the corresponding blood flow. Thus, we allowed this parameter to vary regionally within the

lungs, and in each ROI, t_{delay}, k_1, k_2, k_3, and F_B were simultaneously estimated by fitting the model to the regional ^{18}F-FDG kinetics using an iterative optimization technique.[17] In order to compare parameter estimates between the models with and without the delay, we also fit each ROI's tracer kinetics with the conventional three-compartment model (i.e., the right heart input function model), which assumes the regional lung plasma input function to be equal to the right heart plasma function ($C_p[t] = C_{RH}[t]$, $t_{delay} = 0$).

Estimation of Regional Perfusion from ^{18}F-FDG Kinetics Parameters

In order to estimate regional perfusion from the parameters of the delayed input function model, we devised a multi-compartment model to describe tracer transport times between the right heart and distinct lung regions (Fig. 2). According to this model, the total delay between the right heart and a given lung ROI i ($t_{delay,i}$) represents the sum of a common pulmonary artery delay (t_{PA}) and a local delay specific to ROI i ($t_{ROI,i}$). The pulmonary artery and each ROI's blood pool were modeled as compartments whose transit dynamics were assumed to be described by the central volume principle, which states that the mean transit time ($\bar{t}_{transit}$) equals the ratio of blood volume (V_B) to blood flow ($\dot{Q}$).

$$\bar{t}_{transit} = \frac{V_B}{\dot{Q}} \quad (1)$$

In order to estimate the delay specific to a given ROI, we first calculated the common pulmonary artery delay t_{PA} using Equation 1 and subtracted it from the total regional delay. The perfusion of the pulmonary artery was assumed to be equal to the measured cardiac output (CO), and its blood volume (V_{PA}) was estimated from animal mass using morphometric data on mammalian vascular dimensions in the literature.[30] Thus,

$$t_{PA} = \frac{V_{PA}}{CO} \quad (2)$$

For each ROI i, t_{PA} was subtracted from the total delay measured from local ^{18}F-FDG kinetics ($t_{delay,i}$) to obtain the ROI-specific delay ($t_{ROI,i}$):

$$t_{ROI,i} = t_{delay,i} - t_{PA} \quad (3)$$

Rearranging Equation 1, the perfusion of ROI i ($\dot{Q}_{ROI,i}$) can be computed from the ROI's delay ($t_{ROI,i}$) and its blood volume ($V_{B,i}$):

$$\dot{Q}_{ROI,i} = \frac{V_{B,i}}{t_{ROI,i}} \quad (4)$$

By substituting $V_{B,i} = F_{B,i} \cdot V_{ROI,i}$, where $F_{B,i}$ is the fractional blood volume of ROI i (estimated from tracer kinetics) and $V_{ROI,i}$ is the total volume of ROI i, we obtain specific perfusion, an index of perfusion per unit volume:

$$\frac{\dot{Q}_{ROI,i}}{V_{ROI,i}} = \frac{F_{B,i}}{t_{ROI,i}} \quad (5)$$

Thus, regional specific perfusion was calculated in each ROI as the ratio of F_B to t_{ROI}. In each animal, values of specific perfusion were mean normalized, providing measurements of relative regional perfusion derived with the delayed input function model ($\dot{Q}_{DIF}$).

Measurement of Regional Perfusion from ^{13}NN Kinetics

In order to compare our estimates of $\dot{Q}_{DIF}$ with those of a reference method, regional perfusion was also estimated in each ROI from the kinetics of infused ^{13}NN. During the apnea period of imaging, ^{13}NN accumulates in aerated regions but passes through non-aerated alveoli. Thus, peak ^{13}NN activity may be used as a measure of the relative perfusion to a lung region.[11, 38] Measurements of peak regional ^{13}NN concentration were mean normalized in each animal to obtain ^{13}NN–based measurements of relative perfusion ($\dot{Q}_{REF}$).

Statistical Analysis

Data are presented as mean ± standard deviation unless otherwise noted. Physiological variables were compared between groups using a Student's t test for normally distributed data or a Wilcoxon signed rank test otherwise. Delay estimates were compared using a two-way ANOVA with group and region-of-interest as independent variables and Tukey-Kramer correction for multiple comparisons. Linear correlations were quantified with the Pearson coefficient. Model goodness-of-fit for the delayed input function and right heart input function models was quantified with the Akaike Information Criterion (AIC), which provides a measure of the balance between accurate description of data and minimization of the number of model parameters.[1, 19, 32] AIC values for the two models were compared using a Student's t test. Parameter estimates for the two models were compared by examining the percent differences between delayed input function model parameter estimates (P_{DIF}) and those of the right heart input function model (P_{RHIF}), where P denotes a given ^{18}F-FDG kinetics parameter, using the equation:

$$\%\text{difference} = \frac{P_{RHIF} - P_{DIF}}{P_{DIF}} \cdot 100\% \quad (6)$$

All statistical analyses were performed with Matlab (MATLAB R2012a Statistics Toolbox, The Mathworks, Natick, MA). Significance was set at $p<0.05$.

Results

Physiology and Animal Model

As per design, the Control group was ventilated with significantly lower tidal volumes, PEEP, and F_IO_2, and higher respiratory rates than the Lung Injury group (Table 1). The Lung Injury group showed oxygenation within the range defined for ARDS

(P_aO_2/F_iO_2<200), while the Control group tended to have higher oxygenation. Cardiac output was significantly higher in the Control group.

Estimates of Regional Delay in ^{18}F-FDG Kinetics

Comparison of the early (0–2 minute) right heart tracer kinetics with pulmonary kinetics in distinct isogravitational ROIs (Fig. 3) revealed clear temporal differences between tracer arrival in the right heart and subsequent arrival in the lung. By accounting for this delay at the regional level, the delayed input function model allowed for improved description of the early kinetics, with the predicted local tracer arrival in the plasma coinciding much more closely with the initial increase in tracer activity observed in the lung ROIs (Fig. 3c-d).

Delays between the right heart and the lung ROIs estimated with the delayed input function model (t_{delay}) ranged from 2.0–13.6 s, averaging 6.4±2.9 s. The component of this delay attributed to the pulmonary artery transit time (t_{PA}) averaged 0.90±0.22 s for all animals studied, and was slightly higher (p=0.049) in the Lung Injury group (0.97±0.27 s) than in the Control group (0.82±0.15 s), likely due to hemodynamic differences between the groups (see Table 1). After subtracting the pulmonary artery component from the total delays, we found ROI-specific delays (t_{ROI}) ranging from 1.2–12.8 s for all ROIs studied, with an average of 5.5±2.9 s. These delays showed a significant dependence (p<0.001) on ROI gravitational position (Fig. 4), with non-dependent regions having higher delays than middle or dependent regions in all three studied lung conditions. There were no significant differences in t_{ROI} between the control (4.8±2.4 s), LPS (5.6±3.3 s), or Lavage + LPS (6.1±2.9 s) conditions.

Model Goodness-of-Fit

The delayed input function model yielded lower AIC values than the right heart input function model (p<0.001) in 98.1% (53 out of 54) of the studied ROIs (Fig. 5a). The difference in AIC between the models ($AIC_{RHIF} - AIC_{DIF}$) was positively correlated (r = 0.44, p<0.001) with the magnitude of the estimated delay (Fig. 5b). These findings imply a substantial improvement in description of the data by including t_{delay} as a model parameter, particularly in regions where a large delay was observed.

Differences in ^{18}F-FDG Kinetics Parameters between Models

Parameters describing the transport and trapping of ^{18}F-FDG in the lung demonstrated significant differences between the delayed input function model and the right heart input function model (Fig. 6). Linear regressions between parameters of the two models revealed significant deviations from the line of identity, particularly for parameters k_1, k_2, and F_B, implying systematic differences in parameter estimates between the models (see Table S1, Online Resource 1 for details). This was confirmed by the percent differences in right heart input function model parameter estimates relative to those of the delayed input function model, which were dependent on the parameter and specific lung condition (Table 2). The right heart input function model yielded substantially higher estimates of parameters k_1 and k_2 relative to the delayed input function model, which resulted in slightly higher values of F_e and K_i in most conditions (Table 2). The right heart input function model also yielded lower estimates of ^{18}F-FDG phosphorylation rate k_3 in the Control group and higher estimates of

k_3 in both Lung Injury conditions, while fractional blood volume F_B was lower in all conditions with this model. The parameters k_1, k_2, and F_B, which are particularly relevant to the description of the early (<5 min) ^{18}F-FDG kinetics, showed the largest discrepancies between the models, whereas k_3, F_e, and K_i, which determine mainly the later (>5 min) ^{18}F-FDG kinetics, showed smaller differences between models.

Blood Flow Parameters Derived from ^{18}F-FDG Kinetics

Measurements of relative regional perfusion derived from parameter estimates of the delayed input function model were strongly correlated with measurements of perfusion obtained from ^{13}NN imaging (Fig. 7a). The best-fit lines relating the two sets of perfusion estimates had slopes that were not significantly different from 1, and intercepts not different from 0, in all three studied conditions. Both techniques detected a significant dependence of perfusion on ROI gravitational position ($p<0.001$), with highest perfusion in dependent regions according to both techniques. Considering the ^{13}NN perfusion estimates as a reference, there was no systematic relation between error in $\dot{Q}_{DIF}$ and perfusion magnitude in any group (see Fig. S1, Online Resource 2).

Regional estimates of mean-normalized fractional blood volume as well as the transport delay were also associated with the reference perfusion measurements (Fig. 7b,c). Interestingly, while blood volume showed a strong linear association with perfusion, the intercept of this relation was significantly greater than 0, implying the presence of a positive lung blood volume in the absence of flow (Fig. 7b). The slopes of the F_B vs. $\dot{Q}_{REF}$ regression lines were smaller than 1 in all conditions. In addition, we found significant associations between the inverse of the local delays (t_{ROI}^{-1}) and $\dot{Q}_{REF}$, as would be expected from Equation 4.

When smaller regions were studied by dividing the lungs along the gravitational axis into a greater number of ROIs, the correlation coefficient between perfusion estimates of the two techniques decreased for all three studied lung conditions (see Fig. S2, Online Resource 2). Thus, for smaller ROIs, perfusion estimates obtained with the delayed input function model showed a weaker but still acceptable agreement with the reference method, implying a slight reduction in perfusion measurement accuracy with decreasing ROI size. The smallest ROI size studied was close to 50 mL, below which regional ^{18}F-FDG kinetics became noisier and the model did not reliably converge.

Discussion

In this study, we propose an approach for modeling pulmonary ^{18}F-FDG kinetics that includes an input function delay to account for tracer transport between the site of plasma function measurement (i.e., the right heart) and the plasma pool of the model ROI (i.e., the regional pulmonary capillary blood pool). By applying this technique in sheep models of healthy and injured lung conditions, we found that: (1) the delayed input function model provided significant improvements in description of ^{18}F-FDG kinetics, with lower AIC values justifying the increased model complexity in 98% of studied regions; (2) vascular transport delays between the right heart and the lung range from 2.0–13.6 s and average 6.4 s, with highest values in gravitationally non-dependent regions; (3) ^{18}F-FDG kinetics

parameters k_1, k_2, and F_B, which derive mainly from the early phase of kinetics, were different between the two models in all conditions studied; and (4) parameters derived with the delayed input function model provided measurements of relative regional perfusion that were highly correlated with those of an established ^{13}NN perfusion imaging technique.

The calibration of image-derived input functions to account for temporal delays and dispersion is a topic that has received considerable attention in PET imaging of myocardial perfusion[16, 24] and cerebral perfusion[37] and metabolism.[12, 45] However, applications in pulmonary imaging have been limited to ^{15}O-H_2O-PET of pulmonary perfusion, and input function delays have not been considered in pulmonary ^{18}F-FDG-PET studies.[4, 23, 32-34] In this study, we demonstrate clear differences in tracer arrival time between the right heart and the lungs following the start of ^{18}F-FDG infusion, which emphasize the need for an input function delay in modeling pulmonary ^{18}F-FDG kinetics. Thus, we modified the three-compartment model to include a unique input function delay in each lung region.

Lung-specific delays estimated with our model are closely related to pulmonary capillary transit times. In gravitationally distinct regions, we found lung-specific delays ranging from 1.2–12.8 seconds, with longest delays in non-dependent regions. Interestingly, Wagner et al. found a similar range of vertically dependent pulmonary capillary transit times in dogs of similar weight to our studied sheep, averaging 12.3 s in non-dependent regions and 1.6 s in dependent regions.[41] In rats, capillary transit times showed a comparable range between 1.3 and 12.3 s, and were also dependent on blood flow.[27] These consistent magnitudes, vertical trends, and flow dependence of pulmonary transit times between those studies and our data support the use of the delayed input function model to estimate regional pulmonary vascular transit times.

We chose to use the Akaike Information Criterion to compare the two models of ^{18}F-FDG kinetics. This statistical criterion is based on the concept of minimizing both the average error between model prediction and data as well as the number of model parameters.[1, 19] Thus, the delayed input function model received a penalty for its additional parameter, t_{delay}. In spite of this, we found lower AIC values in 53 out of 54 ROIs, suggesting that including the delay as a model parameter results in an overall improvement of model quality that justifies the additional parameter. Also, the positive relationship between the difference in AIC between models and the magnitude of the local lung delay suggests that errors in the prediction of early ^{18}F-FDG kinetics by the right heart input function model were dependent on the size of the delay itself. This finding is consistent with theoretical expectations, as the early kinetics of a region with a large delay would be poorly described by the plasma function of the right heart, since the tracer would arrive much earlier in the right heart than in the microcirculation of the lung. In such conditions, allowing a shift of the right heart plasma function in time should significantly improve the model description of local kinetics, a presumption directly supported by our data.

We found important differences between ^{18}F-FDG kinetics parameters estimated with the delayed input function and right heart input function models. The right heart input function model yielded significantly lower estimates of F_B and higher estimates of k_1 and k_2. These parameters describe the blood pool size and the transfer of tracer between plasma and tissue,

and are associated with the description of the early stages of ^{18}F-FDG kinetics. We did not find major differences between the models for K_i, F_e, and k_3, consistent with previous evidence that K_i measurements in the brain are relatively insensitive to the input function.[12] While we were not able to compare parameter estimates of each model to a gold-standard method, the improved accuracy of the delayed input function model estimates of k_1, k_2, and F_B is supported by two key findings: (1) improved description of ^{18}F-FDG kinetics with this model (as indicated by lower AIC values); and (2) accuracy of perfusion estimates, which were computed from the F_B and t_{delay} parameters of the model. Because the right heart input function model does not provide estimates of t_{delay} (i.e., it is assumed to be 0), it is not possible to derive perfusion estimates with this model for comparison, as the denominator of Equation 5 would equal zero.

These observed differences in kinetic parameter estimates may have implications for the interpretation of ^{18}F-FDG-PET studies. For example, the parameter blood volume (F_B), for which we found a small but systematic underestimation when the input function delay was ignored, was recently proposed by Pouzot et al. as a useful surrogate for regional perfusion.[26] However, because their method only estimates relative and not absolute perfusion, and the F_B values between the models were highly correlated (r=0.99), the incorporation of the input function delay in their approach may not afford any improvement in precision. Importantly, we found no major differences between models in the parameters K_i, F_e, and k_3, which have been used in several studies to assess regional inflammatory cell activity.[5-7, 15, 18, 34, 44] Given the recent evidence of the relevance of K_i, F_e, and k_3 to investigate the early stages of lung injury,[7, 8, 44] this finding indicates that use of a three-compartment model without the input function delay is acceptable if these are the primary parameters of interest. However, future studies interested in measurements of k_1, k_2, or F_B should consider using the delayed input function model to improve parameter accuracy.

Our measurements of relative perfusion derived with the delayed input function model showed strong linear associations with measurements of perfusion based on the ^{13}NN-saline technique, an established method validated against gas exchange measurements.[20, 22, 34, 38, 39] The robust agreement between these techniques was supported by several findings, including (1) best-fit lines comparing the two techniques not different from the line of identity; (2) no relationship between measurement differences and perfusion magnitude; and (3) reasonable limits of agreement (see Fig. S1, Online Resource 2). We also found that the agreement between the two techniques decreased when ROI size was reduced (see Fig. S2, Online Resource 2). Presumably, this finding was related to decreased signal-to-noise ratios in smaller ROIs, such that parameter accuracy was reduced in smaller ROIs, a trend previously described for PET-based measurements.[42]

The relation between blood volume and perfusion measurements revealed a strong linear association with positive intercepts and slopes less than 1 in all conditions. The finding of a positive intercept is consistent with the concept of mean circulatory filling pressure,[13] in which a positive pressure and blood volume are observed in the circulation following interruption of the cardiac output. Fuld et al. also observed the presence of a positive intercept of blood volume for zero flow using CT-based measurements of pulmonary blood flow and blood volume.[10] In contrast, Pouzot et al. found a negligible intercept when

comparing ^{18}F-FDG derived blood volume with ^{15}O-H_2O perfusion,[26] which is inconsistent with that physiological principle of mean circulatory filling pressure. This discrepancy could be related to the underestimation of blood volume by Pouzot et al. in consequence of their non-consideration of the delay, as shown in the current work, and supports the relevance of considering a delay for improved physiological description. Contrary to the suggestion of Pouzot et al. that pulmonary transit times are homogeneous throughout the lungs,[26] regional pulmonary vascular delays in our study were highly heterogeneous, in agreement with numerous previous studies on the distributions of pulmonary capillary transit times.[3, 27, 40, 41] Overall, these findings suggest that while blood volume may be correlated with perfusion in most lung conditions, more accurate quantification of perfusion can be achieved by additionally accounting for regional transit times, according to Equation 4.

Parameters provided by the delayed input function model may be useful for new clinical applications of pulmonary ^{18}F-FDG-PET. The ability to simultaneously obtain measurements of regional lung perfusion and metabolism with a single PET scan may facilitate future investigations of acute lung injury, wherein both perfusion and metabolism may show important and related changes.[6] Additionally, the technique may be useful for applications in oncology. For example, Miles et al. showed that the relationships between tumor blood flow and metabolism in non-small cell lung cancer depend on tumor size and stage.[21] Also, Bernstine et al. recently showed that time-to-peak measurements derived from early ^{18}F-FDG kinetics are better than standardized uptake value for discriminating hepatocellular carcinomas from background liver tissue.[2] Thus, simultaneous measurement of regional lung perfusion, delay times, and metabolism could be used for the grading of lung cancers based on tumor functional properties.

Some limitations of the delayed input function model are worth noting. First, the model requires an estimate of the cardiac output, which may not be available in all clinical or research applications. Nonetheless, cardiac output may be estimated from body surface area with reasonable accuracy,[9] and errors in cardiac output do not have a substantial effect on delay estimates (see Online Resource 3). Another limitation is that inclusion of the additional parameter t_{delay} adds uncertainty to parameter estimates. Below ROI sizes of about 50 ml, corresponding to 12 ROIs in each animal, we were not able to reliably achieve model convergence in all ROIs, with some returning non-physiologic parameter values. Thus, the resolution of regions that can be studied with the model is limited by the noise present in ^{18}F-FDG kinetics. It is possible that improved signal-to-noise ratio with newer PET scanners, motion correction, or higher ^{18}F-FDG doses would allow for smaller ROIs to be studied. The uncertainty associated with an additional parameter may also preclude the application of more complex compartmental models, such as the four-compartment model,[32] since increasing numbers of parameters can have an undesirable effect on model convergence and parameter accuracy. Extension of the input function delay to other compartmental models will require further study and validation.

Our experimental approach could be improved by optimizing the ^{18}F-FDG infusion and imaging protocol to better capture early ^{18}F-FDG kinetics. Because our early PET frames were 10 s each, we relied on linear interpolation between the frames to estimate the delay with sub-second resolution. The accuracy of delay estimates could potentially be improved

by using PET frames on the order of 2.5 s during the first minutes of imaging when the ^{18}F-FDG arrives in the right heart and lungs, limiting the effect of errors due to interpolation. Nonetheless, the favorable comparison of lung-specific delays with previously published pulmonary capillary transit times,[41] together with the accuracy of perfusion measurements based on estimated delays, suggest that interpolation errors were likely negligible in this study. Additionally, use of a bolus infusion may provide a better signal from which to estimate the difference in tracer arrival between the right heart and the lungs. We used a moderate rate of tracer infusion (approximately 1.3 ml/s), as this was the fastest pump setting available.

In conclusion, we have developed a new model of pulmonary ^{18}F-FDG kinetics which accounts for delays in tracer arrival in the lungs relative to the site of plasma activity measurement. The model provides estimates of vascular transport delays between the right heart and distinct lung regions, and allows for significant improvements in prediction of ^{18}F-FDG kinetics and in parameter estimation, justifying the use of the model over simpler models. Additionally, measurements of perfusion derived from the model parameters are highly accurate based on comparisons with an established ^{13}NN-saline PET technique. The proposed method can be applied during routine clinical imaging by acquiring dynamic PET images and fitting the model to the imaged ^{18}F-FDG kinetics in order to obtain simultaneous measurements of pulmonary transit times, perfusion, and inflammation with a single protocol.

Supplementary Material

Refer to Web version on PubMed Central for supplementary material.

Acknowledgments

This work was supported by grants R01-HL121228 and R01-HL086827 from the National Heart, Lung, and Blood Institute. The authors declare that they have no conflicts of interest. Two authors (T. Winkler and M. F. Vidal Melo) have a patent related to the computation of the image-derived input function used in the study.

References

1. Akaike H. A new look at the statistical model identification. IEEE Trans Autom Control. 1974; 19:716–723.
2. Bernstine H, Braun M, Yefremov N, Lamash Y, Carmi R, Stern D, Steinmetz A, Sosna J, Groshar D. FDG PET/CT early dynamic blood flow and late standardized uptake value determination in hepatocellular carcinoma. Radiology. 2011; 260:503–510. [PubMed: 21555347]
3. Capen RL, Hanson WL, Latham LP, Dawson CA, Wagner WW Jr. Distribution of pulmonary capillary transit times in recruited networks. J Appl Physiol (1985). 1990; 69:473–478. [PubMed: 2228856]
4. Chen DL, Mintun MA, Schuster DP. Comparison of methods to quantitate 18F-FDG uptake with PET during experimental acute lung injury. J Nucl Med. 2004; 45:1583–1590. [PubMed: 15347728]
5. Chen DL, Schuster DP. Positron emission tomography with [18F]fluorodeoxyglucose to evaluate neutrophil kinetics during acute lung injury. Am J Physiol Lung Cell Mol Physiol. 2004; 286:L834–40. [PubMed: 14660487]
6. Costa EL, Musch G, Winkler T, Schroeder T, Harris RS, Jones HA, Venegas JG, Vidal Melo MF. Mild endotoxemia during mechanical ventilation produces spatially heterogeneous pulmonary neutrophilic inflammation in sheep. Anesthesiology. 2010; 112:658–669. [PubMed: 20179503]

7. de Prost N, Costa EL, Wellman T, Musch G, Tucci MR, Winkler T, Harris RS, Venegas J, Kavanagh B, Vidal Melo MF. Effects of Ventilation Strategy on Distribution of Lung Inflammatory Cell Activity. Crit Care. 2013; 17:R175. [PubMed: 23947920]
8. de Prost N, Costa EL, Wellman T, Musch G, Winkler T, Tucci MR, Harris RS, Venegas JG, Vidal Melo MF. Effects of surfactant depletion on regional pulmonary metabolic activity during mechanical ventilation. J Appl Physiol. 2011; 111:1249–1258. [PubMed: 21799132]
9. de Simone G, Devereux RB, Daniels SR, Mureddu G, Roman MJ, Kimball TR, Greco R, Witt S, Contaldo F. Stroke volume and cardiac output in normotensive children and adults. Assessment of relations with body size and impact of overweight. Circulation. 1997; 95:1837–1843. [PubMed: 9107171]
10. Fuld MK, Halaweish AF, Haynes SE, Divekar AA, Guo J, Hoffman EA. Pulmonary perfused blood volume with dual-energy CT as surrogate for pulmonary perfusion assessed with dynamic multidetector CT. Radiology. 2013; 267:747–756. [PubMed: 23192773]
11. Galletti GG, Venegas JG. Tracer kinetic model of regional pulmonary function using positron emission tomography. J Appl Physiol. 2002; 93:1104–1114. [PubMed: 12183508]
12. Guo H, Renaut RA, Chen K. An input function estimation method for FDG-PET human brain studies. Nucl Med Biol. 2007; 34:483–492. [PubMed: 17591548]
13. Guyton AC, Polizo D, Armstrong GG. Mean circulatory filling pressure measured immediately after cessation of heart pumping. Am J Physiol. 1954; 179:261–267. [PubMed: 13218155]
14. Harris RS, Willey-Courand DB, Head CA, Galletti GG, Call DM, Venegas JG. Regional VA, Q, and VA/Q during PLV: effects of nitroprusside and inhaled nitric oxide. J Appl Physiol. 2002; 92:297–312. [PubMed: 11744673]
15. Hartwig W, Carter EA, Jimenez RE, Jones R, Fischman AJ, Fernandez-Del Castillo C, Warshaw AL. Neutrophil metabolic activity but not neutrophil sequestration reflects the development of pancreatitis-associated lung injury. Crit Care Med. 2002; 30:2075–2082. [PubMed: 12352044]
16. Herrero P, Hartman JJ, Senneff MJ, Bergmann SR. Effects of time discrepancies between input and myocardial time-activity curves on estimates of regional myocardial perfusion with PET. J Nucl Med. 1994; 35:558–566. [PubMed: 8151375]
17. Huyer W, Neumaier A. Global Optimization by Multilevel Coordinate Search. J Glob Optim. 1999; 14:331–355.
18. Jones HA, Clark RJ, Rhodes CG, Schofield JB, Krausz T, Haslett C. In vivo measurement of neutrophil activity in experimental lung inflammation. Am J Respir Crit Care Med. 1994; 149:1635–1639. [PubMed: 7516252]
19. Landaw EM, DiStefano JJ 3rd. Multiexponential, multicompartmental, and noncompartmental modeling. II. Data analysis and statistical considerations. Am J Physiol. 1984; 246:R665–77. [PubMed: 6720989]
20. Melo MF, Harris RS, Layfield JD, Venegas JG. Topographic basis of bimodal ventilation-perfusion distributions during bronchoconstriction in sheep. Am J Respir Crit Care Med. 2005; 171:714–721. [PubMed: 15640360]
21. Miles KA, Griffiths MR, Keith CJ. Blood flow-metabolic relationships are dependent on tumour size in non-small cell lung cancer: a study using quantitative contrast-enhanced computer tomography and positron emission tomography. Eur J Nucl Med Mol Imaging. 2006; 33:22–28. [PubMed: 16180030]
22. Musch G, Layfield JD, Harris RS, Melo MF, Winkler T, Callahan RJ, Fischman AJ, Venegas JG. Topographical distribution of pulmonary perfusion and ventilation, assessed by PET in supine and prone humans. J Appl Physiol. 2002; 93:1841–1851. [PubMed: 12381773]
23. Musch G, Venegas JG, Bellani G, Winkler T, Schroeder T, Petersen B, Harris RS, Melo MF. Regional gas exchange and cellular metabolic activity in ventilator-induced lung injury. Anesthesiology. 2007; 106:723–735. [PubMed: 17413910]
24. Pajevic S, Bacharach SL, Carson RE, Weiss GH. Effects of time delay in cardiac blood flow measurements by bolus H2(15)O. IEEE Trans Med Imaging. 1997; 16:294–300. [PubMed: 9184891]

25. Patlak CS, Blasberg RG, Fenstermacher JD. Graphical evaluation of blood-to-brain transfer constants from multiple-time uptake data. J Cereb Blood Flow Metab. 1983; 3:1–7. [PubMed: 6822610]
26. Pouzot C, Richard JC, Gros A, Costes N, Lavenne F, Le Bars D, Guerin C. Noninvasive quantitative assessment of pulmonary blood flow with 18F-FDG PET. J Nucl Med. 2013; 54:1653–1660. [PubMed: 23907755]
27. Presson RG Jr, Todoran TM, De Witt BJ, McMurtry IF, Wagner WW Jr. Capillary recruitment and transit time in the rat lung. J Appl Physiol (1985). 1997; 83:543–549. [PubMed: 9262451]
28. Rhodes CG, Wollmer P, Fazio F, Jones T. Quantitative measurement of regional extravascular lung density using positron emission and transmission tomography. J Comput Assist Tomogr. 1981; 5:783–791. [PubMed: 6976359]
29. Richard JC, Janier M, Decailliot F, Le Bars D, Lavenne F, Berthier V, Lionnet M, Cinotti L, Annat G, Guerin C. Comparison of PET with radioactive microspheres to assess pulmonary blood flow. J Nucl Med. 2002; 43:1063–1071. [PubMed: 12163633]
30. Sackner MA, Atkins N, Goldberg J, Segel N, Zarzecki S, Wanner A. Pulmonary arterial blood volume and tissue volume in man and dog. Circ Res. 1974; 34:761–769. [PubMed: 4598994]
31. Saha D, Takahashi K, de Prost N, Winkler T, Pinilla-Vera M, Baron RM, Vidal Melo MF. Micro-Autoradiographic Assessment of Cell Types Contributing to 2-Deoxy-2-[(18)F]Fluoro-D-: Glucose Uptake During Ventilator-Induced and Endotoxemic Lung Injury. Mol Imaging Biol. 2012
32. Schroeder T, Vidal Melo MF, Musch G, Harris RS, Venegas JG, Winkler T. Modeling Pulmonary Kinetics of 2-Deoxy-2-[(18)F]fluoro-d-glucose During Acute Lung Injury. Acad Radiol. 2008; 15:763–775. [PubMed: 18486012]
33. Schroeder T, Vidal Melo MF, Musch G, Harris RS, Venegas JG, Winkler T. Image-derived input function for assessment of 18F-FDG uptake by the inflamed lung. J Nucl Med. 2007; 48:1889–1896. [PubMed: 17942803]
34. Schroeder T, Vidal Melo MF, Musch G, Harris RS, Winkler T, Venegas JG. PET Imaging of Regional 18F-FDG Uptake and Lung Function After Cigarette Smoke Inhalation. J Nucl Med. 2007; 48:413–419. [PubMed: 17332619]
35. Sergiacomi G, Bolacchi F, Cadioli M, Angeli ML, Fucci F, Crusco S, Rogliani P, Pezzuto G, Romeo F, Mariano E, Simonetti G. Combined pulmonary fibrosis and emphysema: 3D time-resolved MR angiographic evaluation of pulmonary arterial mean transit time and time to peak enhancement. Radiology. 2010; 254:601–608. [PubMed: 20093531]
36. Sokoloff L, Reivich M, Kennedy C, Des Rosiers MH, Patlak CS, Pettigrew KD, Sakurada O, Shinohara M. The [14C]deoxyglucose method for the measurement of local cerebral glucose utilization: theory, procedure, and normal values in the conscious and anesthetized albino rat. J Neurochem. 1977; 28:897–916. [PubMed: 864466]
37. van den Hoff J, Burchert W, Muller-Schauenburg W, Meyer GJ, Hundeshagen H. Accurate local blood flow measurements with dynamic PET: fast determination of input function delay and dispersion by multilinear minimization. J Nucl Med. 1993; 34:1770–1777. [PubMed: 8410297]
38. Vidal Melo MF, Layfield D, Harris RS, O'Neill K, Musch G, Richter T, Winkler T, Fischman AJ, Venegas JG. Quantification of regional ventilation-perfusion ratios with PET. J Nucl Med. 2003; 44:1982–1991. [PubMed: 14660725]
39. Vidal Melo MF, Winkler T, Harris RS, Musch G, Greene RE, Venegas JG. Spatial heterogeneity of lung perfusion assessed with (13)N PET as a vascular biomarker in chronic obstructive pulmonary disease. J Nucl Med. 2010; 51:57–65. [PubMed: 20008987]
40. Wagner WW Jr, Latham LP, Gillespie MN, Guenther JP, Capen RL. Direct measurement of pulmonary capillary transit times. Science. 1982; 218:379–381. [PubMed: 7123237]
41. Wagner WW Jr, Latham LP, Hanson WL, Hofmeister SE, Capen RL. Vertical gradient of pulmonary capillary transit times. J Appl Physiol (1985). 1986; 61:1270–1274. [PubMed: 3781943]
42. Wellman TJ, Winkler T, Costa EL, Musch G, Harris RS, Venegas JG, Melo MF. Measurement of Regional Specific Lung Volume Change Using Respiratory-Gated PET of Inhaled 13N-Nitrogen. J Nucl Med. 2010; 51:646–653. [PubMed: 20237036]

43. Wellman TJ, Winkler T, Costa EL, Musch G, Harris RS, Venegas JG, Vidal Melo MF. Effect of regional lung inflation on ventilation heterogeneity at different length scales during mechanical ventilation of normal sheep lungs. J Appl Physiol. 2012; 113:947–957. [PubMed: 22678958]

44. Wellman TJ, Winkler T, Costa EL, Musch G, Harris RS, Zheng H, Venegas JG, Vidal Melo MF. Effect of local tidal lung strain on inflammation in normal and lipopolysaccharide-exposed sheep*. Crit Care Med. 2014; 42:e491–500. [PubMed: 24758890]

45. Zanotti-Fregonara P, Fadaili el M, Maroy R, Comtat C, Souloumiac A, Jan S, Ribeiro MJ, Gaura V, Bar-Hen A, Trebossen R. Comparison of eight methods for the estimation of the image-derived input function in dynamic [(18)F]-FDG PET human brain studies. J Cereb Blood Flow Metab. 2009; 29:1825–1835. [PubMed: 19584890]

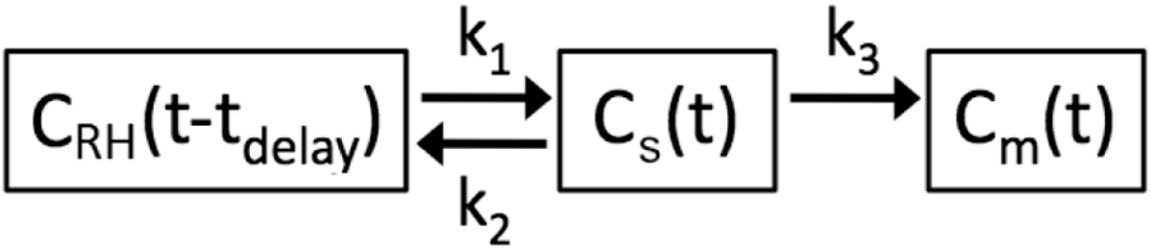

Fig. 1.

The delayed input function model used to describe regional lung ^{18}F-FDG kinetics. Rate constants k_1 and k_2 describe the transfer of ^{18}F-FDG between blood in the pulmonary capillary blood pool, whose activity is represented by a time delay of the right heart plasma concentration ($C_{RH}[t-t_{delay}]$), and the extravascular substrate compartment ($C_s[t]$). The parameter t_{delay}, which is unique to this model, represents the time required for ^{18}F-FDG to travel from the right heart to the local pulmonary capillary blood pool, while k_3 describes the rate of transfer into the metabolized compartment ($C_m[t]$), representing intracellular phosphorylation of ^{18}F-FDG. The fractional blood volume (F_B, not shown) is an additional model parameter

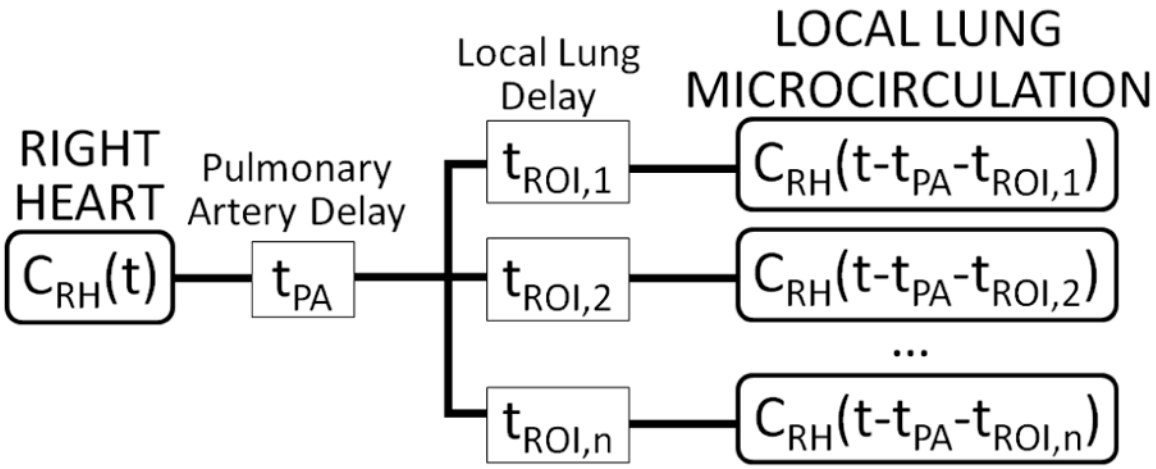

Fig. 2.

Schematic of time delays in ^{18}F-FDG transport between the right heart and the local lung microcirculation (i.e., capillary blood pool). ^{18}F-FDG activity vs. time in the right heart, $C_{RH}(t)$, is measured using dynamic imaging of a region-of-interest (ROI) drawn over the right heart.[33] We included a common delay in ^{18}F-FDG transport associated with transit through the pulmonary artery (t_{PA}), as well as local delays specific to each ROI i ($t_{ROI,i}$), the sum of which determined the total local delay i ($t_{delay,i} = t_{PA} + t_{ROI,i}$). For each ROI, $t_{delay,i}$ was estimated from local ^{18}F-FDG kinetics with the delayed input function model (Fig. 1)

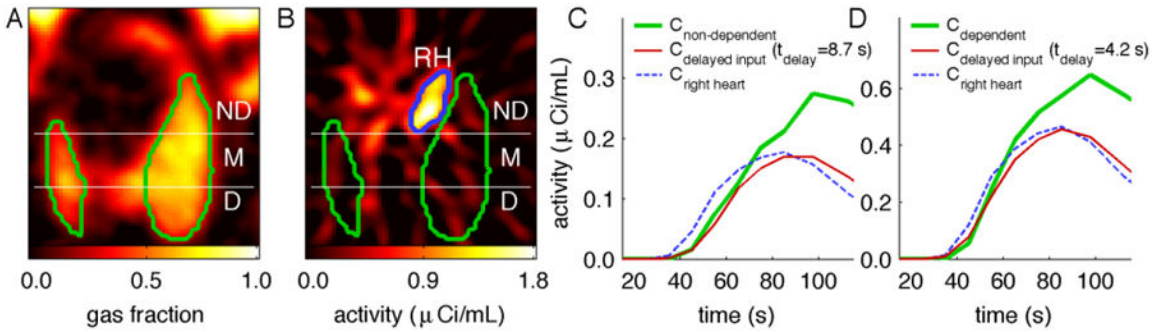

Fig. 3.

(a) Representative image of regional gas fraction in the lung, with non-dependent (ND), middle (M), and dependent (D) regions-of-interest shown within the imaged lung field (outlined in green). (b) ^{18}F-FDG activity within the first minute of tracer infusion: ^{18}F-FDG is clearly visible within the right heart (RH, outlined in blue) but not yet distinguishable in the lung. (c,d) The delay required for tracer transport from the right heart to the lungs was evident in the early (<2 min) tracer kinetics, as the activity in the right heart (blue dashed lines) began to rise earlier than the activity in non-dependent (c) or dependent (d) lung regions (green lines). By accounting for tracer transport delays through inclusion of a delay of the right heart plasma function as a model parameter (t_{delay}), the delayed plasma function in the ROIs (red lines) coincided much more closely with the initial rise in activity of those regions

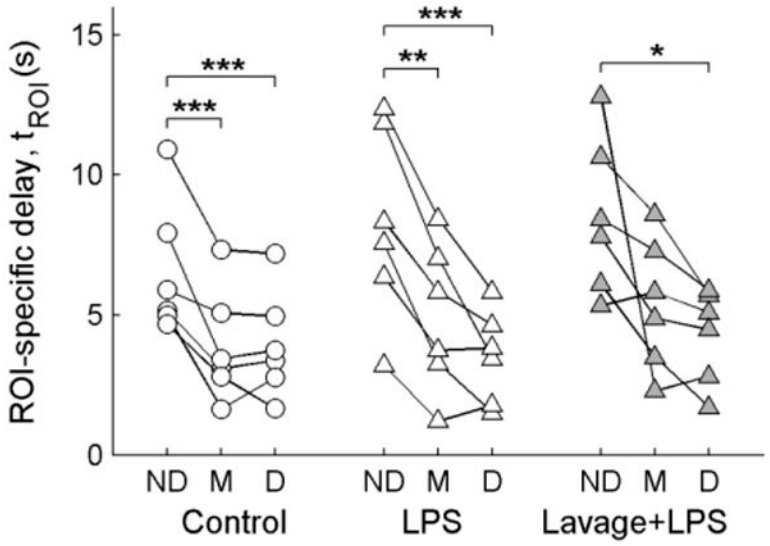

Fig. 4.

Distributions of ROI-specific delays derived with the delayed input function model. ROI delays (t_{ROI}) were computed by subtracting the pulmonary artery delay (t_{PA}) from the total delay estimated from regional ^{18}F-FDG kinetics (t_{delay}), according to Equation 3. A significant dependence of t_{ROI} on gravitational position was found ($p<0.001$), with the non-dependent (ND) regions showing higher delays than the middle (M) or dependent (D) regions in post-hoc tests. No significant differences were found between the Control, LPS, or Lavage + LPS conditions. *$p<0.05$, **$p<0.01$, ***$p<0.001$

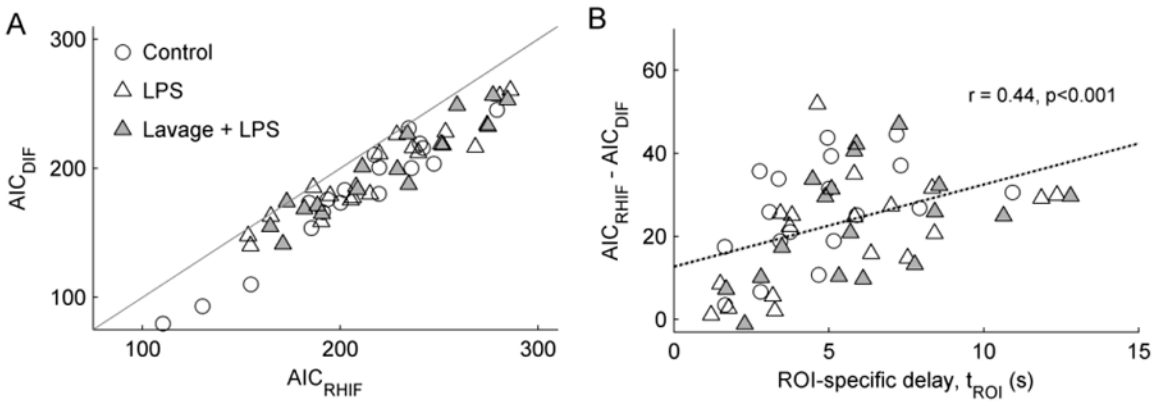

Fig. 5.

(a) Comparison of the Akaike Information Criterion (AIC) for the delayed input function (AIC_{DIF}) and right heart input function (AIC_{RHIF}) models. Lower AIC values imply better description of the data for the number of model parameters. AIC_{DIF} was lower than AIC_{RHIF} (i.e., below the identity line) in 53 of 54 studied regions-of-interest. (b) Model improvement with the delayed input function, defined as the difference in AIC between the two models, was significantly correlated with the magnitude of ROI delays (t_{ROI})

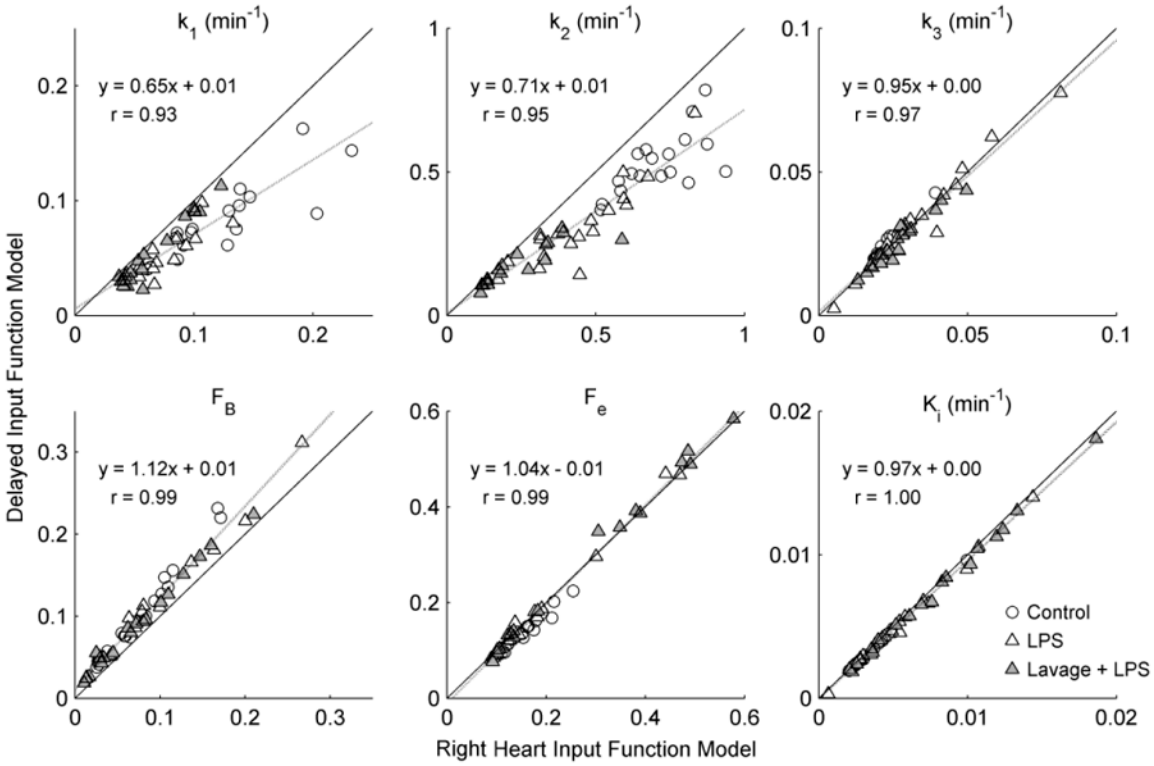

Fig. 6.

Comparison of ^{18}F-FDG kinetics parameters estimated with the delayed input function and right heart input function models. Substantial differences between the models were observed for the parameters k_1, k_2, and F_B, which are primarily determined by the early phase of ^{18}F-FDG kinetics. The ^{18}F-FDG net uptake rate K_i, phosphorylation rate k_3, and volume of distribution F_e, were quite similar between the models, as data fell close to the line of identity

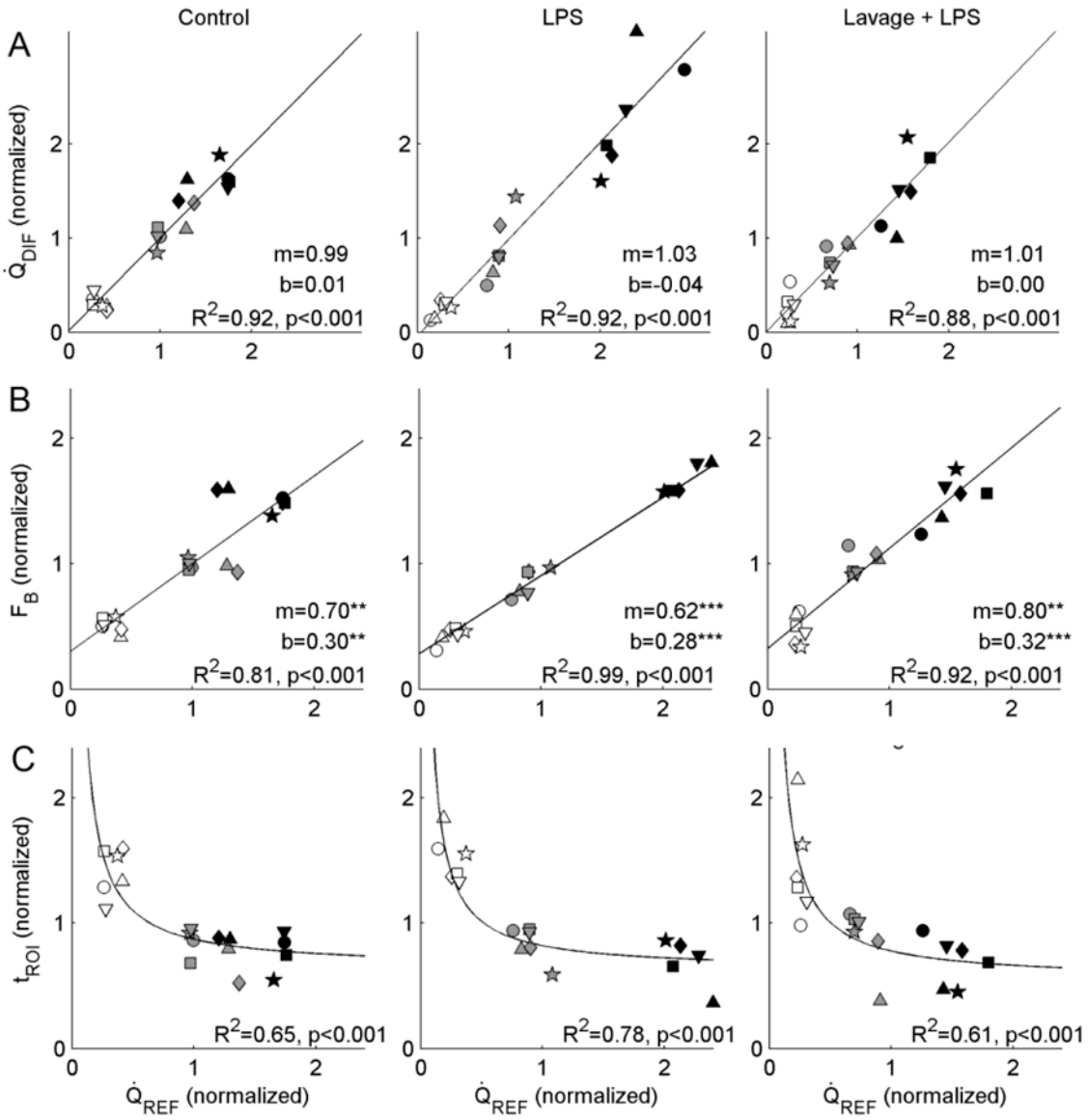

Fig. 7.

(a) Regional perfusion estimated using the delayed input function model parameters ($\dot{Q}_{DIF}$) compared with the ^{13}NN-saline reference method ($\dot{Q}_{REF}$). Data within each animal were mean-normalized, and are shown with distinct symbols. In all three groups, we found strong correlations between the two measurements, with regression lines not significantly different from the line of identity either in terms of slope or intercept. According to both techniques, perfusion was dependent on ROI gravitational position ($p<0.001$), with non-dependent regions (empty symbols) showing lower perfusion than middle (gray) or dependent regions (black). (b) Mean-normalized fractional blood volume (F_B) was also correlated with $\dot{Q}_{REF}$, though the regression lines differed from the line of identity in terms of both slope and intercept for all three conditions. Of note, the positive intercepts in all groups imply the presence of a residual blood volume when perfusion is equal to zero. (c) Local lung delays

(t_{ROI}) were inversely associated with $\dot{Q}_{REF}$ in all groups, with regions of higher perfusion showing shorter delays. Curves show regression of t_{ROI} onto $\dot{Q}_{REF}$

Table 1
Weight and Cardiorespiratory Variables

	Control (0 h)	Injury (4 h)
Weight, kg	22.6 ± 2.4	20.8 ± 0.9
V_T, $mLkg^{-1}$	8.7 ± 0.9	11.8 ± 2.7 *
PEEP, cmH_2O	0.0 ± 0.0	9.0 ± 1.1 ***
RR, bpm	26.0 ± 2.5	20.7 ± 3.9 *
F_IO_2	0.33 ± 0.08	0.68 ± 0.12 ***
CO, $L{\cdot}min^{-1}$	5.4 ± 1.1	3.7 ± 0.7 *
MAP, mmHg	94.0 ± 8.6	83.8 ± 23.3
MPAP, mmHg	13.2 ± 4.6	34.3 ± 5.3 ***
P_aO_2/F_iO_2, torr	274 (229–284)	130 (72–159) #
P_aCO_2, torr	32.5 ± 4.4	39.3 ± 3.4 *

V_T, tidal volume; PEEP, positive end-expiratory pressure; RR, respiratory rate; F_IO_2, inspired O_2 fraction; CO, cardiac output; MAP, mean arterial pressure; MPAP, mean pulmonary arterial pressure; P_aO_2, arterial O_2 pressure; P_aCO_2, arterial CO_2 pressure;

# p<0.10,

* p<0.05,

** p<0.01,

*** p<0.001 vs. Control

Table 2

Percent Differences in ^{18}F-FDG Parameter Estimates for the Right Heart Input Function Model Relative to the Delayed Input Function Model

	Control	LPS	Lavage + LPS
k_1	43.1 [31.0,61.8]^{b}	50.3 [28.3,65.3]^{b}	17.9 [9.8,34.0]^{b,c}
k_2	33.0 [23.0,46.4]^{b}	46.8 [18.8,62.1]^{b}	25.9 [10.8,35.4]^{b}
k_3	-5.1 [-9.2,-2.9]^{b,d}	0.7 [-6.4,14.1]	3.9 [1.2,9.0]^{a}
F_B	-27.0 [-33.1,-21.2]^{b}	-22.9 [-35.1,-17.3]^{b}	-18.2 [-31.3,-13.9]^{b}
F_e	9.5 [8.1,15.1]^{b,d}	2.9 [0.6,9.0]^{a}	-1.8 [-4.1,0.9]
K_i	5.1 [3.6,5.9]^{b}	2.9 [2.0,11.3]^{b}	4.4 [2.2,6.3]^{b}

Shown are median [25th, 75th percentiles] for % error.

^{a} $p<0.05$,

^{b} $p<0.01$ for null hypothesis that difference is equal to 0;

^{c} $p<0.05$,

^{d} $p<0.01$ vs. both other groups